Comput. Methods Appl. Mech. Engrg. 197 (2008) 4062–4075

Contents lists available at ScienceDirect

Comput. Methods Appl. Mech. Engrg.

journal homepage: www.elsevier.com/locate/cma

A monolithic approach for topology optimization of electrostatically actuated devices

Gil Ho Yoon [a,b,1], Ole Sigmund [b,*]

[a] School of Mechanical Engineering, KyungPook National University, Republic of Korea
[b] Department of Mechanical Engineering, Solid Mechanics, Technical University of Denmark, Denmark

ARTICLE INFO

Article history:
Received 1 November 2007
Received in revised form 23 March 2008
Accepted 5 April 2008
Available online 15 April 2008

Keywords:
Topology optimization
Electrostatics
Monolithic analysis
Continuum mechanics

ABSTRACT

This paper presents a new topology optimization scheme for nonlinear electrostatic systems actuated by Coulomb's forces. For successful optimization, computational issues such as (i) alternating governing equations with respect to spatially defined design variables, (ii) imposing interaction boundary conditions between insulator (air) and conductor (solid) and (iii) control of minimum geometrical feature sizes must be addressed. To address the first two issues, the paper presents a monolithic formulation based on continuum mechanics theory which simultaneously calculates the electric potential and structural displacements. To interpolate between insulator and conductor with continuous design variables, the monolithic approach distinguishes between the permittivity value of the electric Poisson's equation and that of Maxwell's stress tensor. For the optimization, standard material interpolations are used for Young's modulus and permittivity values. Moreover, a recently developed morphology filter is applied to control electrode gaps and other geometrical features.

1. Introduction

It is a challenging task to design multiphysics systems through engineer's intuition because of their complex nature. Therefore, after the introduction of the topology optimization method [1,2], many works have applied it to multiphysics systems, especially in the MEMS application area [3–16]. As an extension of this trend, this paper presents a new computational framework, paving the way for systematic design of nonlinear electrostatic systems actuated by Coulomb's force [17–20].

Electrostatics refers to a simple case of electromagnetism where the electric field is considered quasistatic due to stationary electric charges [21]. Moreover, in an electric field, a structure will be subjected to electrostatic forces due to induced charges on its surfaces. Generally, this electrostatic force can be computed by surface integration of the so-called Maxwell's stress tensor [21,22]. Most of the widely used MEMS devices use this electrostatic phenomenon for actuation. Typical examples are comb-drive actuators and sensors consisting of integrated capacitors [12,18].

Because the movement of a conductor influences the electric field as well as the electrostatic forces, the coupling between the electric field and the structural displacements must be considered simultaneously. In order to analyze electromechanically coupled systems, there exist several computational approaches (see e.g., [7,11]). The principal method is the staggered analysis method which calculates the electric field in the air and the structural displacements of the conductor separately in each subdomain. Depending on strategy, there are several ways of solving the coupled problem [22]. Normally several iterations are required, each involving solution of the respective system possibly using different analysis techniques (e.g., BEM and FEM). On the other hand, monolithic approaches which calculate the two fields simultaneously have been suggested recently [7,8]. Monolithic analysis approaches also require several iterations. However, as opposed to most staggered analysis methods, the monolithic method solves the two fields in a unified domain.

Concerning optimization of electrostatic systems, size and shape optimizations have been carried out by a number of researchers (see [17–19] and references in them). Considering the electric field only, topology optimization has been applied to electrostatic rotors in [12]. Topology optimization of the full electromechanically coupled problem has recently been initiated by four groups [7,11,15,16] using widely different approaches. Ref. [11] suggests a staggered analysis method to design actuators and [7] uses a monolithic approach to maximize the pull-in voltage of structures. Both approaches consider fixed boundaries between air and conductor and hence topological variations are limited to the structural domain. The limitation of design freedom is

* Corresponding author. Tel.: +45 45254256.
E-mail addresses: ghy@knu.ac.kr (G.H. Yoon), Sigmund@mek.dtu.dk (O. Sigmund).

[1] This work was carried out while Gil Ho Yoon was employed at the Technical University of Denmark.

0045-7825/$ - see front matter © 2008 Elsevier B.V. All rights reserved.
doi:10.1016/j.cma.2008.04.004

introduced in order to avoid the problem of defining electrostatic force boundary conditions when the boundaries are unknown a priori as is the case in topology optimization. The interfacing boundary condition issue between two distinct governing equations also arises in topology optimization for pressure load and acoustic-structure interaction problems. In Refs. [5,10], the problem was overcome by interpolation between the PDEs of the two physics problems resulting in a mixed displacement–pressure (**U**–P) formulation. A similar approach can be suggested to avoid the problem with identifying electrostatic force boundary conditions in the topology optimization method. In this paper we elaborate and improve on a fully coupled approach first suggested by us in Ref. [16]. A related approach has recently been suggested for the weakly coupled problem in Ref. [15].

In order to implement a topology optimization scheme for nonlinear electrostatic actuator design problems, this paper suggests a monolithic analysis scheme and changes permittivity and Young's modulus simultaneously in the whole design domain. In doing so, we can resolve the issues of alternating governing equations in air and conductor as well as the identification of the coupling boundary conditions along boundaries between insulator and conductor as shown in Fig. 1.

In the present monolithic approach, continuum mechanics theory plays an important role in deriving the fully-coupled equations [22–24]. For material interpolations, the Young's modulus and permittivity values are interpolated by usual SIMP (Solid Isotropic Material with Penalization) functions with respect to design variables. To simulate perfect conductivities of conductors, we distinguish between the permittivity in Poisson's equation, here named "generalized permittivity", and the permittivity used for the electrostatic force calculation. Based on this idea, we can successfully carry out the topology optimization for electrostatic structures. Moreover, we address some issues of localization of the actuation area in the design domain and filtering techniques that avoid too small and mesh-dependent features.

The paper is organized as follows: Section 2 sets up basic notations for the electric and linear elasticity equations and briefly reviews the standard staggered analysis method. Section 3 presents the monolithic approach formulated in the undeformed domain, provides several analytical examples verifying the method, and compares the results with other methods. Section 4 describes interpolation functions, local optima and implementation. Section 5 presents several examples of topology optimization applied to two-dimensional electrostatic actuators. In Section 6 we summarize our findings and discuss some future research subjects.

2. Governing equations for electrostatic systems and the staggered analysis method

To provide a basis for further derivations, we start by describing the standard staggered approach for solving electromechanically coupled problems. In the subsequent section we modify the modeling scheme to the monolithic formulation.

2.1. Basic notation

To consistently describe the steady-state deformation of structures actuated by Coulomb's forces, we define the relation between coordinates of the undeformed ${}^{0}_{e/s}\Omega$ and deformed ${}^{t}_{e/s}\Omega$ systems by

$$\mathbf{x} = \mathbf{X} + \mathbf{u}, \tag{1}$$

where $\mathbf{x} = \{x_i\}$ and $\mathbf{X} = \{X_i\}$ ($i = 1,2$ for 2D and $i = 1,2,3$ for 3D) are coordinates in the deformed and un-deformed domains, respectively, and the structural deformation is denoted by **u**. Left-subscripts e or s refer to the electric or structural subdomains, respectively (see Fig. 2a). Moreover, we define the differential operators in the deformed and un-deformed domains:

$$\nabla_{\mathbf{X}} = \frac{\partial}{\partial X_i} \quad \text{in} \quad {}^{0}_{e/s}\Omega, \nabla_{\mathbf{x}} = \frac{\partial}{\partial x_i} \quad \text{in} \quad {}^{t}_{e/s}\Omega. \tag{2}$$

The finite deformation tensor, **F**, is defined as the partial differentiation of the current coordinate **x** with respect to the undeformed coordinate **X**. Thereby, the differential operators of the two configurations can be related using the deformation tensor:

$$\mathbf{F} = \frac{\partial \mathbf{x}}{\partial \mathbf{X}}, \quad \nabla_{\mathbf{X}} = \mathbf{F}^{\mathrm{T}} \nabla_{\mathbf{x}}, \quad \nabla_{\mathbf{x}} = \mathbf{F}^{-\mathrm{T}} \nabla_{\mathbf{X}}. \tag{3}$$

2.2. The electrostatic equation

The electric and magnetic fields of general media can be calculated by solving Maxwell's equations [21]. Usually, the two fields are strongly coupled. However, in this research we assume linear and non-magnetic media. Hence the equations can be decoupled and only the electric field needs to be solved for. The considered media have conductivity, σ, and permittivity, ε, where both are arbitrary functions of space:

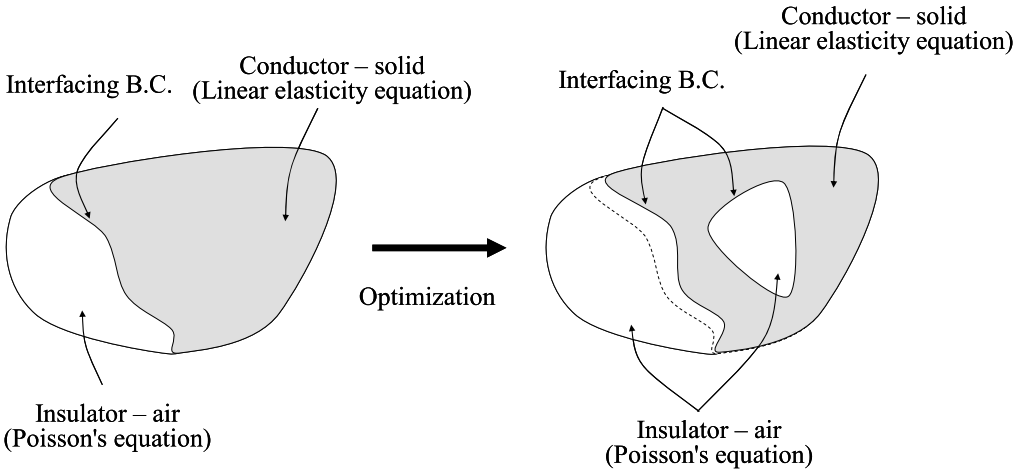

Fig. 1. Alternating governing equations and boundary conditions for electrostatic system. Left: modeling domain consisting of one air domain and one solid domain with interfacing boundary conditions. Right: during optimization the original interaction boundary may change shape and new boundaries must be allowed to form.

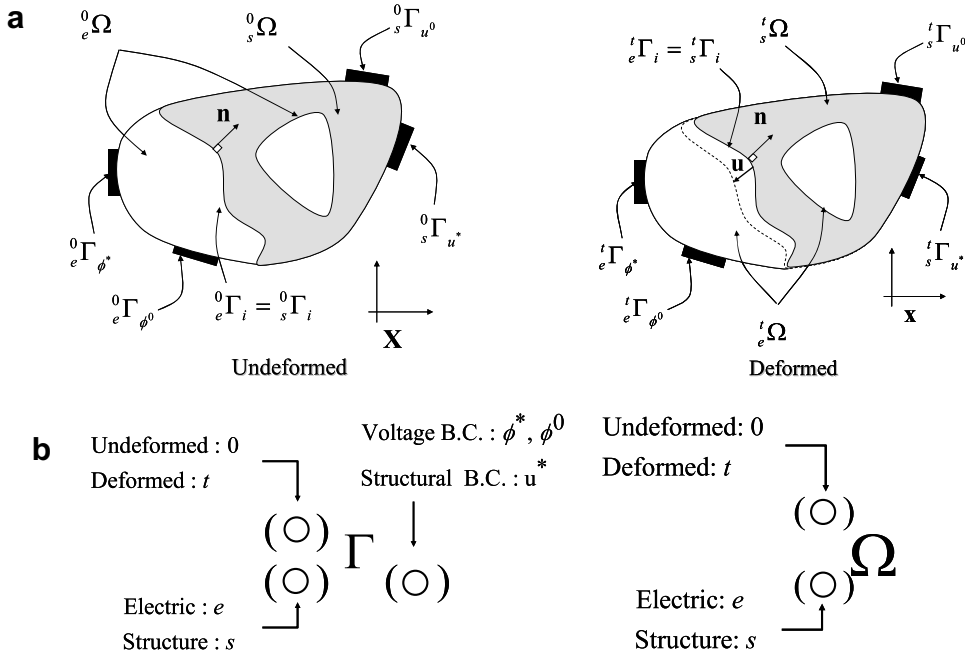

Fig. 2. Notations used in a staggered analysis method. (a) Definitions of boundaries and domains, and (b) illustrations of index notation.

$$\sigma = \sigma(\mathbf{x}), \quad \varepsilon = \varepsilon(\mathbf{x}). \tag{4}$$

Assuming an irrotational electric field, **E**, with a scalar electric potential ϕ ($\mathbf{E} = -\nabla_{\mathbf{x}}\phi$), one may derive the following governing equations [21]:

$$\text{Equation of continuity} : \nabla_{\mathbf{x}} \cdot (\sigma \mathbf{E}) + \frac{\partial \rho}{\partial t} = 0 \quad \text{and}$$
$$\text{Gauss law} : \nabla_{\mathbf{x}} \cdot (\varepsilon \mathbf{E}) = \rho, \tag{5}$$

where the charge density is denoted by ρ [21]. Coupling of these two equations results in the following transient equation defined in the deformed domain ${}^t_e\Omega$ (see Fig. 2 for notations for boundaries and domains):

$$\text{General equation} : \nabla_{\mathbf{x}} \cdot \left(\sigma \mathbf{E} + \frac{\partial}{\partial t} \varepsilon \mathbf{E} \right) = 0 \quad \text{or}$$
$$\nabla_{\mathbf{x}} \cdot \left(\sigma \nabla_{\mathbf{x}} \phi + \frac{\partial}{\partial t} \varepsilon \nabla_{\mathbf{x}} \phi \right) = 0 \quad \text{in} \quad {}^t_e\Omega. \tag{6}$$

The transient Eq. (6) can be solved in order to calculate electric fields in media with a given permittivity and non-zero conductivity. It is, however, common to degenerate this transient system into a static equation with either conductivity or permittivity depending on media [21].

In an ideal insulator such as air, the conductivity is assumed to be zero and the following static Poisson's equation with only a spatially varying permittivity must be solved in the deformed domain ${}^t_e\Omega$:

$$\nabla_{\mathbf{x}} \cdot (\varepsilon(\mathbf{x}) \cdot \nabla_{\mathbf{x}} \phi) = 0 \quad \text{in} \quad {}^t_e\Omega(\mathbf{u}). \tag{7}$$

Here, we assume that the external charge is zero.

The boundary conditions are defined as follows:

$$\begin{aligned} &\phi = 0 \quad \text{on} \quad {}^t_e\Gamma_{\phi^0}(\mathbf{u}) : \text{Ground B.C.}, \\ &\phi = \phi^* \quad \text{on} \quad {}^t_e\Gamma_{\phi^*}(\mathbf{u}) : \text{Voltage B.C.}, \\ &\phi = \phi^* \quad \text{on} \quad {}^t_e\Gamma_i(\mathbf{u}) : \text{Interface B.C.}, \end{aligned} \tag{8}$$

where the applied voltage on ${}^t_e\Gamma_{\phi^*}(\mathbf{u})$ is denoted by ϕ^* and the boundary ${}^t_e\Gamma_{\phi^0}(\mathbf{u})$ is grounded. Moreover the interfacing boundary condition ${}^t_e\Gamma_i$ commonly has the voltage boundary condition ϕ^* because the structure is assumed to be an ideal conductor.

Using the principle of virtual work, the weak form of Poisson's equation can be derived:

$$\text{Electric potential equation} : \int_{{}^t_e\Omega} (\nabla_{\mathbf{x}} \delta\phi)^{\mathrm{T}} \cdot \varepsilon(\mathbf{x}) \cdot \nabla_{\mathbf{x}} \phi \, \mathrm{d}\Omega = 0, \tag{9}$$

where $\delta\phi$ denotes the virtual potential.

2.3. Structural equations

Any structure having a permittivity $\varepsilon(\mathbf{x})$ in an electric field is subjected to electrostatic forces on the interfacing boundary ${}^t_s\Gamma_i(\mathbf{u})$ due to the so-called (electric) Maxwell's stress tensor which corresponds to the symmetric 2-Rank stress momentum tensor of an electromagnetic field [21,22]:

$$\mathbf{T}_E = \varepsilon(\mathbf{x}) \left(\mathbf{E}\mathbf{E} - \frac{\mathbf{E} \cdot \mathbf{E}}{2} \mathbf{I} \right) \quad \text{on} \quad {}^t_s\Gamma_i(\mathbf{u}) (= {}^t_s\Gamma_i(\mathbf{u})). \tag{10}$$

The structural equation neglecting body forces can be defined as,

$$\nabla_{\mathbf{x}} \cdot \mathbf{T} = 0 \quad \text{in} \quad {}^t_s\Omega(\mathbf{u}). \tag{11}$$

The boundary conditions are defined:

$$\begin{aligned} &\mathbf{n} \cdot \mathbf{T} = \mathbf{f}_e \quad \text{on} \quad {}^t_s\Gamma_i(\mathbf{u}) \quad (\text{where } \mathbf{n} \text{ is the normal vector}), \\ &\mathbf{u} = \mathbf{u}^* \quad \text{on} \quad {}^t_s\Gamma_{\mathbf{u}^*}, \\ &\mathbf{u} = \mathbf{u}^0 \quad \text{on} \quad {}^t_s\Gamma_{\mathbf{u}^0}. \end{aligned} \tag{12}$$

The Dirichlet boundary conditions are imposed on ${}^t_s\Gamma_{u^*}$ for $\mathbf{u} = \mathbf{u}^*$ and ${}^t_s\Gamma_{\mathbf{u}^0}$ for $\mathbf{u} = \mathbf{u}^0$, respectively, and the Neumann boundary condition is imposed on ${}^t_s\Gamma_i(\mathbf{u})$.

The electrostatic traction force $\mathbf{f}_e$, the strain **S**, and the stress **T**, are defined as Eqs. (13) and (14):

$$\mathbf{S} = \frac{1}{2} (\nabla_{\mathbf{x}}^{\mathrm{T}} \mathbf{u} + \nabla_{\mathbf{x}} \mathbf{u}), \quad \mathbf{T} = \mathbf{C}\mathbf{S}, \tag{13}$$
$$\mathbf{f}_e = \mathbf{n} \cdot \mathbf{T}_E \quad \text{on} \quad {}^t_s\Gamma_i(\mathbf{u}) (= {}^t_e\Gamma_i(\mathbf{u})). \tag{14}$$

Here, we assume geometrically linear strains, **S**, calculated from the current displacements, **u**. The Cauchy stress is denoted by **T** and the deformation-independent constitutive matrix is denoted by **C**.

Using the principle of virtual work, the following equation can be derived:

$$\text{Linear elasticity equation}: \int_{{}^{t}_{s}\Omega} \delta \mathbf{S}^{\mathrm{T}} \mathbf{T} \mathrm{d}\Omega = -\int_{{}^{t}_{s}\Gamma_i} \delta \mathbf{u}^{\mathrm{T}} \mathbf{f}_{\mathrm{e}} \mathrm{d}\Gamma, \tag{15}$$

where the virtual displacements and associated virtual strains are denoted by $\delta\mathbf{u}$ and $\delta\mathbf{S}$, respectively.

In deriving this equation, some important assumptions were used. First of all, we assume *geometrically linear analysis*. In other words, we neglect changes of surface areas, volumes and mass densities between the undeformed and the deformed structural domains [23]. Due to this assumption, the 2nd Piola–Kirchhoff stress and the Cauchy stress measures become identical. Furthermore, the associated strain measures – the Green–Lagrangian strain and the linear strain – also become identical when assuming deformation independent material properties. Thus, the elasticity equation is simplified to

$$\underbrace{\int_{{}^{0}_{s}\Omega} \delta \mathbf{S}^{\mathrm{T}} \mathbf{T} \mathrm{d}\Omega}_{\substack{\text{Geometrically linear} \\ (\nabla_{\mathbf{x}} \equiv \nabla_{\mathbf{X}})}} = \underbrace{-\int_{{}^{t}_{s}\Gamma_i} \delta \mathbf{u}^{\mathrm{T}} \mathbf{f}_{\mathrm{e}}(\phi(\mathbf{u}), \mathbf{u}) \mathrm{d}\Gamma}_{\substack{\text{Deformation dependent load} \\ (\nabla_{\mathbf{x}} \neq \nabla_{\mathbf{X}})}}. \tag{16}$$

Here, the elasticity equation is simply calculated in the undeformed domain and the differential operators of the undeformed and deformed systems can be treated as the same operator, i.e., $\nabla_{\mathbf{x}} \equiv \nabla_{\mathbf{X}}$. However, the right term of Eq. (15) is dependent on displacements and is a so-called *deformation dependent load* [23]. Therefore, the geometry due to the current displacements $\mathbf{u}$ should be considered. Unlike the left-hand side, the differential operators of the deformed and the un-deformed systems are treated differently, i.e.,$\nabla_{\mathbf{x}} \neq \nabla_{\mathbf{X}}$ (see p. 528 of [23] for more details).

2.4. Staggered analysis method

The governing equation for the electric field (9) as well as the right-hand-side of the elasticity Eq. (16) are defined in the deformed configuration which is a function of the displacements ($\mathbf{u}$). Therefore, the electric potential and the structural displacements must be solved iteratively through the so-called staggered analysis method as illustrated in Fig. 3. Normally, after solving the electric field, the electrostatic force associated with that electric field is calculated through surface integration of Maxwell's stress tensor. Then the pure structural equation is solved with the calculated electrostatic force using Eq. (16). These steps should be repeated until both fields have converged.

The accuracy of the staggered analysis method is dependent on how the electric potential equation of Eq. (9) is solved in the deformed electric domain ${}^{t}_{e}\Omega(\mathbf{u})$. The key step is obtaining an update geometry, ${}^{t}_{e}\Omega(\mathbf{u})$, considering the current structural displacements $\mathbf{u}$ from Eq. (16). There are two common approaches to update the geometry: (1) Generating a completely new mesh for ${}^{t}_{e}\Omega(\mathbf{u})$ while maintaining the boundaries between the structural and electrostatic domains or (2) keeping the original mesh and adjusting the locations of existing nodes by morphing an original mesh or by solving a simple elasticity equation for ${}^{t}_{e}\Omega(\mathbf{u})$. In both cases, additional computations are required [22].

The staggered approach with either remeshing or morphing is in general use and works well for size and shape optimization problems. Moreover, it is a computationally robust and efficient method which is being used in state-of-the-art commercial softwares such as ANSYS [22]. Unfortunately, this staggered analysis method does not allow for free material redistribution in connection with topology optimization because (i) it requires an explicit interfacing boundary description for the coupling boundary conditions, (ii) depending on design variable values, two governing equations must be alternated between, and (iii) there is an ambiguity for intermediate design variables. In conclusion, there is a need for a scheme that inherits the simplicity and efficiency of staggered methods but at the same time allows for topology optimization without explicit interfacing boundary between insulator and conductor.

3. A fully coupled formulation for electromechanical systems

In the following, we present a new monolithic analysis scheme using the same governing equations as before but defined on the

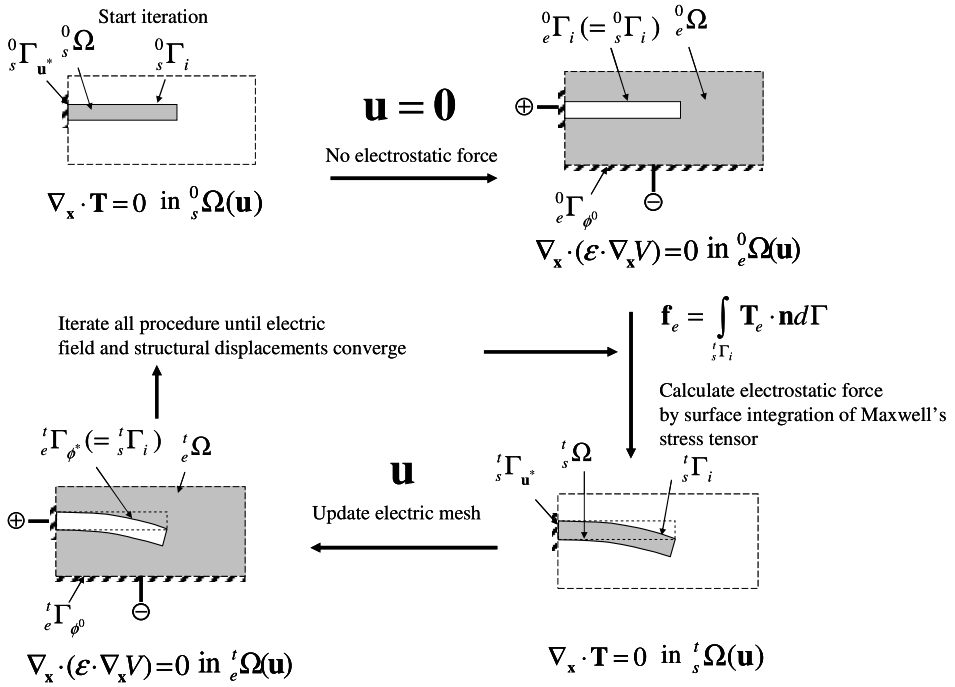

Fig. 3. Computational procedure for the staggered analysis method.

whole analysis domain as shown in Fig. 4. Unlike the staggered analysis method, the electric and mechanical fields are modeled in a unified domain. All previously defined notations are valid except the notations for domain and boundary conditions shown in Fig. 5. The differences compared to the staggered analysis method can be listed as

1. Unified equations for conductor and insulator.
2. A generalized permittivity for solutions of the transient Eq. (6) in the whole domain.
3. Maxwell's stress tensor formulated in domains not on boundaries making use of Gauss's theorem.
4. Transformation of governing equations from the deformed domain to the undeformed domain using the deformation tensor (i.e., no remeshing required).

As opposed to the staggered analysis method, the suggested monolithic approach distinguishes between conductor (e.g., silicon) and insulator (e.g., air), not by changing governing equations from the electric equation to the linear elasticity equation and vice versa, but by changing three material properties in the unified domain (Young's modulus and permittivities in the electric equation and the electrostatic force calculation, respectively). Therefore, a standard topology optimization can be carried out using standard SIMP material interpolation functions for the three material properties. Concerning the second aspect above, the electric field in Eq. (6) must be simulated for both conductor and insulator simultaneously. For the conductor, equal potential conditions must hold for its surfaces. In order to satisfy this condition, we change the transient system Eq. (6) into a static one by introducing a generalized permittivity discussed below. Concerning aspect 3, the electrostatic force is calculated by a volume integration instead of a surface integration of Maxwell's stress tensor because of the non-existing explicit boundary description. Concerning the last aspect, the electric field and the forces are formulated in the undeformed domain. As opposed to the staggered analysis method, we do not want to update an existing mesh or generate a new mesh because this will cause problems for the free material distribution. Therefore, by the help of continuum theory, we formulate the governing equations and electrostatic forces in the undeformed domain.

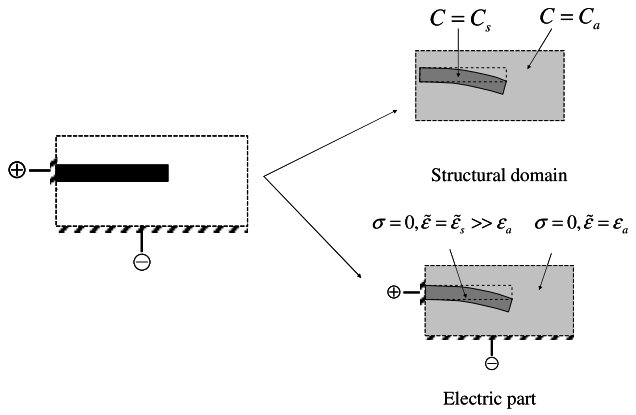

Fig. 4. The present monolithic approach where $\tilde{\varepsilon}$ is the generalized Permittivity used in the electric potential equation, $\tilde{\varepsilon}_s$ the value in solid domains. Young's modulus becomes a very small C_a in the electric domain and the value of the conducting material C_S in the solid domain.

3.1. Generalized permittivity for the electric equation

In order to simulate the electric field of the transient Eq. (6) using a static equation, we propose to use an approximation theory for Eq. (6), described in Refs. [21,25]. Employing a time constant T, the time derivative of the charge density in Eq. (5) can be linearly approximated as,

$$\frac{\partial \rho}{\partial t} \approx \frac{{}^t\rho - {}^0\rho}{T} \quad ({}^0\rho = 0), \tag{17}$$

where ${}^t\rho$ and ${}^0\rho$ are electric charges in the deformed and the undeformed domains, respectively. Ideally, T should be much larger than the material relaxation time, $\tau = \varepsilon/\sigma$ but normally T is selected to be only 100–1000 times larger than τ in order to prevent numerical ill-conditioning [25]. Eq. (6) may now be reformulated in the form:

$$\nabla_{\mathbf{x}} \cdot (\sigma \mathbf{E}) + \frac{\nabla_{\mathbf{x}} \cdot (\varepsilon \mathbf{E})}{T} = 0 \quad \text{or} \quad \nabla_{\mathbf{x}} \cdot (T\sigma + \varepsilon) \nabla_{\mathbf{x}} \phi = 0 \quad \text{in} \quad {}^t\Omega. \tag{18}$$

For a simpler description, we introduce the *generalized permittivity*, $\tilde{\varepsilon}$:

$$\tilde{\varepsilon} \equiv T\sigma + \varepsilon \quad \text{then} \quad \nabla_{\mathbf{x}} \cdot (\tilde{\varepsilon}) \nabla_{\mathbf{x}} \phi = 0 \quad \text{in} \quad {}^t\Omega \tag{19}$$

$$T \gg \tau = \varepsilon/\sigma \quad \text{where} \quad T = \alpha \tau_{\,c} = \alpha \varepsilon_c / \sigma_c, \alpha \gg 1, \tag{20}$$

where the material properties for conductor are denoted by ε_c and σ_c and α is a large constant (=100–1000).

The generalized permittivity $\tilde{\varepsilon}$ for conductor and insulator is defined as,

$$\tilde{\varepsilon} = \begin{cases} \varepsilon_a & \text{inside air,} \\ \tilde{\varepsilon}_s & \text{inside conductor.} \end{cases} \tag{21}$$

Ideally, $\tilde{\varepsilon}_s$ should be an infinite number to satisfy the conditions of a conductor. However, a very high number produces numerical instability. Numerical tests suggest a value around 10^5 times larger than the permittivity of air in order to satisfy the equal potential condition and without causing ill-conditioning. Note that the generalized permittivity should be used only in the electric field equation and not in the evaluation of Maxwell's stress tensor.

3.2. Monolithic formulation in the undeformed domain

Using the generalized permittivity, we can set up the electric equation as,

$$\nabla_{\mathbf{x}} \cdot (\tilde{\varepsilon}(\mathbf{x}) \cdot \nabla_{\mathbf{x}} \phi) = 0 \quad \text{in} \quad {}^t\Omega(\mathbf{u}), \tag{22}$$

where the following boundary conditions are assumed:

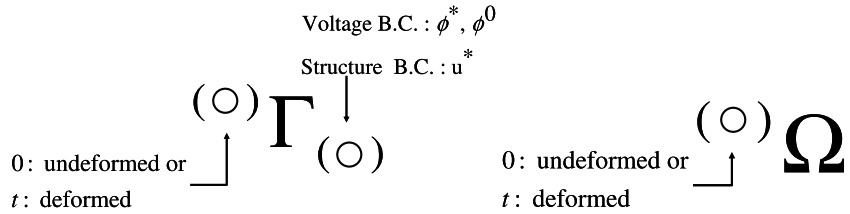

Fig. 5. Notations used in the present monolithic approach. Note that the mechanical domain ${}^{(\circ)}_{s}\Omega$ and the electric domain ${}^{(\circ)}_{e}\Omega$ are identical to ${}^{(\circ)}\Omega(\mathbf{u})$ in this monolithic approach where $\circ$ = "0" means undeformed space and "t" deformed space.

$$\phi = 0 \quad \text{on} \quad {}^t\Gamma_{\phi^0}(\mathbf{u}), \tag{23}$$

$$\phi = \phi^* \quad \text{on} \quad {}^t\Gamma_{\phi^*}(\mathbf{u}). \tag{24}$$

In the monolithic approach, calculating the electrostatic force by surface integration is inadequate because new holes with a priori unknown boundary curves may emerge and disappear during the optimization process. Therefore, we propose to use volume integration of Maxwell's stress tensor to calculate the electrostatic force rather than surface integration:

$$\int_{{}^t\Omega} \mathbf{f}_e \mathrm{d}\Omega = \underbrace{\int_{{}^t\Omega} \nabla_{\mathbf{x}} \cdot \mathbf{T}_E \mathrm{d}\Omega}_{\substack{\text{Present} \\ \text{monolithic approach}}} = \underbrace{\int_{{}^t\Gamma_i} \mathbf{n}^{\mathrm{T}} \mathbf{T}_E \mathrm{d}\Gamma}_{\text{Staggered approach}}. \tag{25}$$

Now we can write the linear elasticity equation including prestress from the Maxwell's stress tensor:

$$\nabla_{\mathbf{x}} \cdot \mathbf{T} + \nabla_{\mathbf{x}} \cdot \mathbf{T}_E = 0 \quad \text{in} \quad {}^t\Omega(\mathbf{u}), \tag{26}$$

$$\mathbf{u} = \mathbf{u}^* \quad \text{on} \quad {}^t\Gamma_{u^*}, \tag{27}$$

$$\mathbf{S} = \frac{1}{2}(\nabla_{\mathbf{x}}^{\mathrm{T}}\mathbf{u} + \nabla_{\mathbf{x}}\mathbf{u}), \quad \mathbf{T} = \mathbf{C}\mathbf{S}. \tag{28}$$

Using the principle of virtual work, the two governing equations in the deformed domain can be set up as,

$$\int_{{}^t\Omega} (\nabla_{\mathbf{x}}\delta\phi)^{\mathrm{T}} \cdot \tilde{\varepsilon}(\mathbf{x}) \cdot \nabla_{\mathbf{x}}\phi \mathrm{d}\Omega = 0, \tag{29}$$

$$\int_{{}^0\Omega} \delta\mathbf{S}^{\mathrm{T}} \cdot \mathbf{T} \mathrm{d}\Omega = -\int_{{}^t\Omega} \delta\mathbf{S}(\mathbf{u}, \delta\mathbf{u})^{\mathrm{T}} \cdot \mathbf{T}_E \mathrm{d}\Omega, \tag{30}$$

where $\delta\mathbf{S} = \frac{1}{2}(\nabla_{\mathbf{X}}\delta\mathbf{u}^{\mathrm{T}} + \nabla_{\mathbf{X}}\delta\mathbf{u})$ and

$$\delta\mathbf{S}(\mathbf{u}, \delta\mathbf{u}) = \frac{1}{2}((\mathbf{F}^{-\mathrm{T}}\nabla_{\mathbf{X}}\delta\mathbf{u})^{\mathrm{T}} + \mathbf{F}^{-\mathrm{T}}\nabla_{\mathbf{X}}\delta\mathbf{u}). \tag{31}$$

The two Eqs. (29) and (30) are formulated in the deformed domain ${}^t\Omega(\mathbf{u})$ except for the linear structural potential energy as explained in the previous section. Still these two equations contain integrations in ${}^t\Omega(\mathbf{u})$ that require updating of the geometry. To resolve this difficulty, we use transformation of the differential operators. In other words, we transfer the two governing equations from the deformed domain to the undeformed domain using Eqs. (3) and (32):

$$\nabla_{\mathbf{x}}\mathbf{u} = \mathbf{F}^{-\mathrm{T}}\nabla_{\mathbf{X}}\mathbf{u}, \nabla_{\mathbf{x}}\phi = \mathbf{F}^{-\mathrm{T}}\nabla_{\mathbf{X}}\phi, \quad \text{and} \quad \int_{{}^t\Omega}()\mathrm{d}\Omega = \int_{{}^0\Omega}()\|\mathbf{F}\|\mathrm{d}\Omega, \tag{32}$$

$$\text{Electric equation}: \int_{{}^0\Omega} (\nabla_{\mathbf{X}}\delta\phi)^{\mathrm{T}}(\mathbf{F}^{-1} \cdot \tilde{\varepsilon}(\mathbf{x}) \cdot \mathbf{F}^{-\mathrm{T}})\nabla_{\mathbf{X}}\phi\|\mathbf{F}\|\mathrm{d}\Omega = 0, \tag{33}$$

$$\text{Linear elasticity equation}: \int_{{}^0\Omega} \delta\mathbf{S}^{\mathrm{T}} \cdot \mathbf{T} \mathrm{d}\Omega = -\int_{{}^0\Omega} \delta\mathbf{S}(\mathbf{u}, \delta\mathbf{u})^{\mathrm{T}} \cdot \mathbf{T}_E \|\mathbf{F}\| \mathrm{d}\Omega. \tag{34}$$

These two equations are coupled with each other because the deformation tensor $\mathbf{F}$ as well as the virtual strains are functions of displacements $\mathbf{u}$. Note that the equations are valid for general media consisting of ideal conductors and insulators. The interfacing boundary conditions between conductor and insulator are automatically satisfied because we formulate the Maxwell's stress tensor as an initial stress term. Therefore, it is not necessary to manually impose interaction boundary conditions, which is one of the advantages of the proposed scheme.

3.3. Illustrative examples

To prove the correctness and efficiency of the modified governing Eqs. (33) and (34), we consider four simple test examples.

Example 1. *Electrostatic force in a capacitor*

The proposed approach can accurately calculate the electrostatic force through volume integration of the Maxwell's stress tensor in the undeformed domain using Eq. (34).

To illustrate this aspect, we consider the capacitor with a spring in Fig. 6. The distance between the two plates changes from d_0 to $d_0 - u_1 + u_2$ when the voltage ϕ^* is applied to the left electrode. Then, the electrostatic force f_e is calculated using the standard approach:

$$\text{Standard approach}: f_e = \frac{1}{2}\frac{\varepsilon_a(\phi_2 - \phi_1)^2}{(d_0 - u_1 + u_2)^2} \Rightarrow \frac{1}{2}\frac{\varepsilon_a(\phi^*)^2}{(d_0 - u_1)^2}. \tag{35}$$

To derive the well-known Eq. (35) using Eq. (34), the virtual strains $\delta\mathbf{S}$ and $\delta\mathbf{S}(\mathbf{u},\delta\mathbf{u})$ in the deformed domain and the deformation tensor are calculated in the form:

$$\delta\mathbf{S} = \frac{\mathrm{d}\delta u}{\mathrm{d}X}, \delta\mathbf{S}(\mathbf{u}, \delta\mathbf{u}) = \frac{\mathrm{d}\delta u}{\mathrm{d}x}, \quad \mathbf{F} = \frac{\mathrm{d}x}{\mathrm{d}X} = 1 + \frac{\mathrm{d}u}{\mathrm{d}X}. \tag{36}$$

Without loss of generality, we assume linear shape functions for the one-dimensional electric elements. Then the electrostatic force term, corresponding to the right-hand side of Eq. (34), can be derived using

$$\frac{\mathrm{d}\phi}{\mathrm{d}X} = \frac{1}{d_0}[-1, 1]\begin{bmatrix}\phi_1 \\ \phi_2\end{bmatrix}, \quad \mathbf{F} = 1 + \frac{1}{d_0}(u_2 - u_1) \tag{37}$$

and hence

$$\begin{aligned} &\text{Monolithic approach}: \\ &-\int_{{}^0\Omega} \delta\mathbf{S}^{\mathrm{T}}(\mathbf{u}, \delta\mathbf{u})\mathbf{T}_E\|\mathbf{F}\|\mathrm{d}\Omega \\ &= -\int_0^{d_0} \underbrace{[\delta u_1, \delta u_2]\frac{1}{d_0}\begin{bmatrix}-1 \\ 1\end{bmatrix}\frac{\mathrm{d}X}{\mathrm{d}x}}_{\delta\mathbf{S}^{\mathrm{T}}(\mathbf{u},\delta\mathbf{u})} \underbrace{\frac{\varepsilon_a}{2}\left(\frac{\mathrm{d}\phi}{\mathrm{d}X}\right)^2\mathbf{F}^{-2}}_{\mathbf{T}_E} \underbrace{\frac{\mathrm{d}x}{\mathrm{d}X}}_{\|\mathbf{F}\|}\mathrm{d}X \\ &= [\delta u_1, \delta u_2]\frac{\varepsilon_a}{2}\frac{(\phi_2 - \phi_1)^2}{(d_0 - u_1 + u_2)^2}\begin{bmatrix}1 \\ -1\end{bmatrix}. \end{aligned} \tag{38}$$

It is seen that the resulting electrostatic force is the same as the one in (35). This simple example shows two aspects:

1. The electrostatic forces of the deformed structure can be accurately calculated by the volume integration of the Maxwell's stress tensor transformed into the undeformed domain using the deformation tensor if the structural displacements are known.

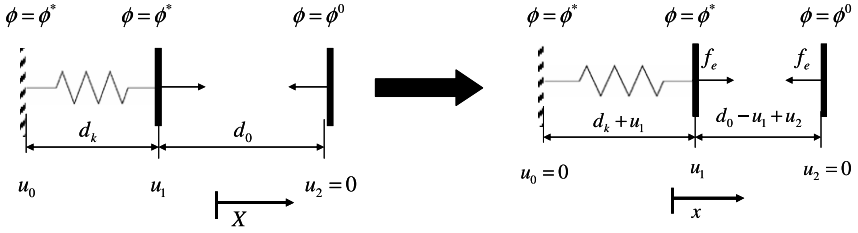

Fig. 6. A general model for forces between parallel plates of a capacitor.

2. The permittivity used in the electrostatic force calculation should be the original permittivity ε_a.

Example 2. *Differential operator transformation*

The proposed approach constructs the electric stiffness matrix but solely based on the structural displacements, without updating the geometry of the electric domain.

To demonstrate this, we consider a simple one-dimensional model consisting of three elements with unit area as seen in Fig. 7. Assuming that the displacements of each node are [0,1,0.5,0], we can calculate the element stiffnesses in Fig. 7b using the standard finite element formulation.

Alternatively, the electric stiffness matrix of the considered one-dimensional system can be calculated using the deformation tensor (left-hand side of Eq. (33)) as shown in Fig. 8:

$$\begin{bmatrix} \phi_1 : \tilde{\varepsilon}_1/2 & -\tilde{\varepsilon}_1/2 & 0 & 0 \\ \phi_2 : -\tilde{\varepsilon}_1/2 & \tilde{\varepsilon}_1/2 + 2\tilde{\varepsilon}_2 & -2\tilde{\varepsilon}_2 & 0 \\ \phi_3 : 0 & -2\tilde{\varepsilon}_2 & 2\tilde{\varepsilon}_2 + 2\tilde{\varepsilon}_3 & -2\tilde{\varepsilon}_3 \\ \phi_4 : 0 & 0 & -2\tilde{\varepsilon}_3 & 2\tilde{\varepsilon}_3 \end{bmatrix}. \tag{39}$$

Using this simple example, we demonstrate how the present monolithic approach can construct the electric stiffness matrix based on structural displacements and without updating the geometry of the electric domain.

Example 3. *A simple capacitor with a spring*

For an electromechanically coupled system, the simplest example having an analytical solution is the capacitor suspended by a spring as shown in Fig. 9. To model this one-dimensional system, a simple two-dimensional model using two rectangular bi-linear 4-node elements is constructed in Fig. 9b. Fig. 10 shows the computed solutions by varying the applied voltage, ϕ^*, as well as the analytical solution given by

$$ku = \frac{1}{2}\varepsilon_a \frac{\phi_{in}^2}{(d_0 - u)^2}, \quad \phi_{cr} = \sqrt{\frac{4}{27} \times \frac{2k}{\varepsilon_a}} \approx 5.4433. \tag{40}$$

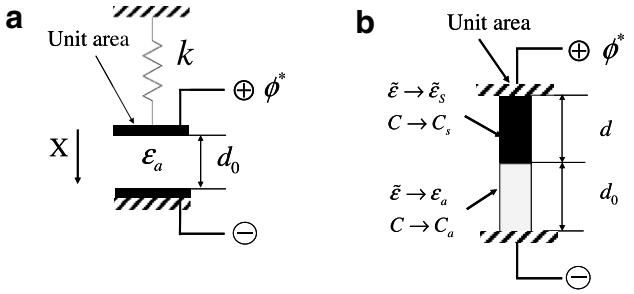

Fig. 9. A capacitor with two parallel plates. (a) An one-dimensional model ($k = 100, d_0 = 0, \varepsilon_a = 1$) and (b) a 2×1 two-dimensional model ($C_s = 100, C_a = C_s \times 10^{-6}, \nu = 0, d_0 = 0, d = 1, \tilde{\varepsilon}_s = 10^5 \varepsilon_a$).

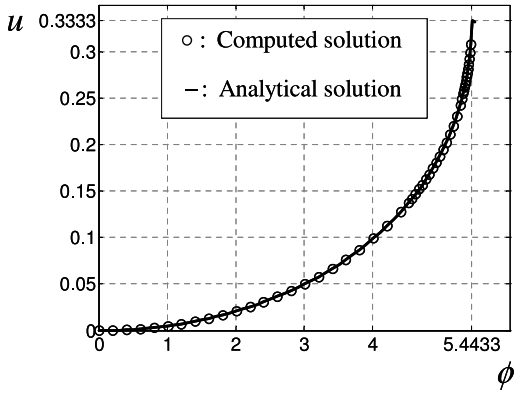

Fig. 10. Numerical results compared with analytical solution for the simple spring suspended capacitor shown in Fig. 9a.

The results are seen to match very well. Near the pull-in voltage $\phi_{cr} = 1/3$, the damped Newton-method used for the numerical computations does not converge because of the near-zero value of the tangent stiffness [7].

Example 4. *Two-dimensional analysis example*

As a last analysis example we compare our solution with solutions computed by the commercial FE software, ANSYS, for the two-dimensional model shown in Fig. 11. The commercial software

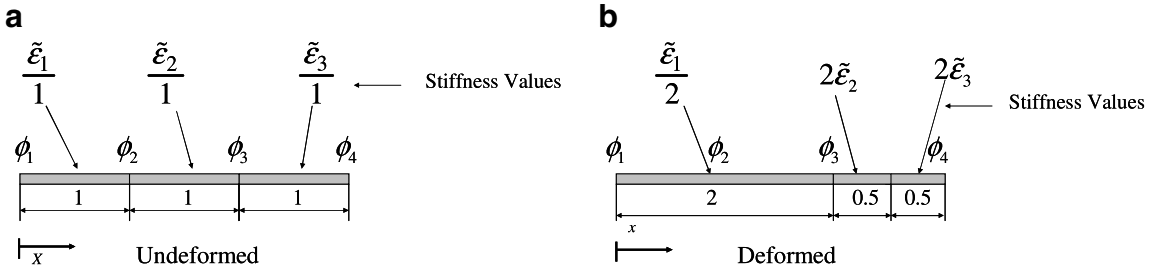

Fig. 7. Calculating electric element stiffnesses for the undeformed and deformed domains, respectively. (a) Stiffness values in the undeformed domain, (b) stiffness values in the deformed domain using the direct method (displacements for each node are (0,1,0.5,0), respectively).

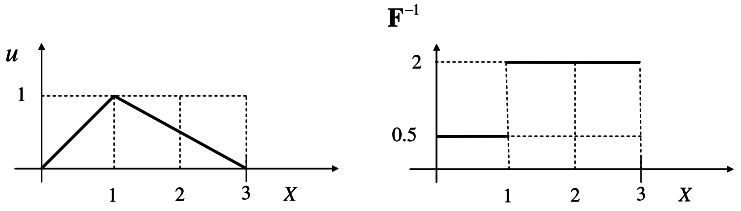

Fig. 8. Displacement field (left) and corresponding deformation tensor (right).

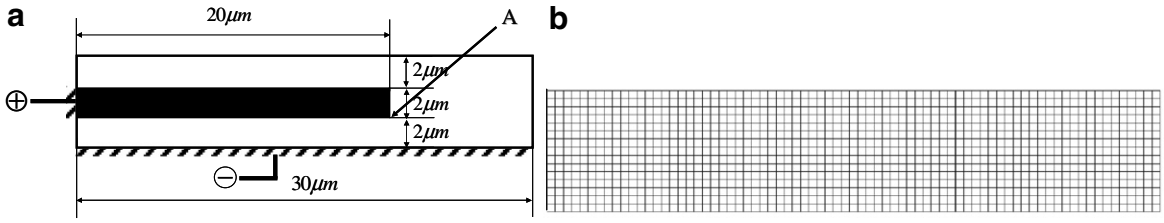

Fig. 11. A simple beam example. (a) Model definition (Young's modulus of solid: 153 GPa, Poisson's ratio of solid: 0.17, relative Permittivity of solid: 10, relative permittivity of air: 1), and (b) finite element mesh.

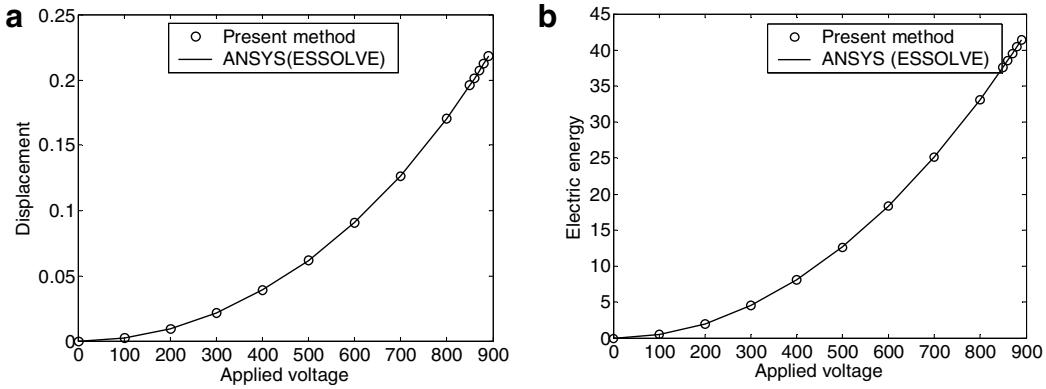

Fig. 12. Responses of Fig. 11. (a) The displacement response at A for varying input potential and (b) the electric energy response.

provides a state-of-the-art subroutine, ESSOLVE, for the solution of electromechanical system using a staggered analysis method. To update the electric domain, it uses a mesh-morphing method with a remeshing method if necessary (see Ref. [22] for more details).

By changing the applied voltage on the supported end of the beam, the vertical displacement at A is calculated with both the present approach and the staggered analysis method provided by ANSYS [22]. Moreover, to check the coupling influence of structural displacements to the electric field, the electric energy π_E of Eq. (41) computed by both methods are compared in Fig. 12b. As shown here, the solutions of the proposed monolithic approach compare very well to the solutions of ANSYS:

$$\pi_E = \frac{1}{2}\int_{\iota\Omega} \mathbf{E}^T \varepsilon(\mathbf{x})\mathbf{E}d\Omega, \quad \mathbf{E} = -\nabla_{\mathbf{x}}\phi = -\mathbf{F}^{-T}\nabla_{\mathbf{X}}\phi. \tag{41}$$

4. Topology optimization formulation

4.1. Interpolation function

For topology optimization, the permittivity for the electrostatic force, the generalized permittivity for the Poisson's equation and Young's modulus are interpolated with respect to design variables γ defined in each element. Using this continuous design variable, two states - conductor and insulator - are interpolated by varying γ between 0 (air) and 1 (conductor). Table 1 summaries the material properties for extreme values of the design variable γ. In the table, C_s and C_a are Young's moduli for solid and void (air), respectively. The permittivity values of solid and void are likewise denoted by ε_s and ε_a, respectively.

In this paper, we use the SIMP (Solid Isotropic Material with Penalization) interpolation functions for the interpolation between air and conductor:

Table 1
Material properties as functions of design variables

	Linear elasticity equation		Electric equation
	Young's modulus (C)	Permittivity (ε)	Generalized permittivity ($\tilde{\varepsilon}$)
Solid ($\gamma = 1$)	C_s	ε_s	$\tilde{\varepsilon}_s \gg \varepsilon_a$
Air ($\gamma = 0$)	C_a	ε_a	ε_a

$$\varepsilon(\gamma) = (\varepsilon_s - \varepsilon_a)\gamma^n + \varepsilon_a, \tag{42}$$

$$C(\gamma) = (C_s - C_a)\gamma^n + C_a, \tag{43}$$

$$\tilde{\varepsilon}(\gamma) = (\tilde{\varepsilon}_s - \varepsilon_a)\gamma^n + \varepsilon_a. \tag{44}$$

The same penalty n is used for each interpolation function. It is important that the penalization term for the electrostatic force (i.e., the permittivity $\varepsilon(\gamma)$) and the generalized permittivity $\tilde{\varepsilon}(\gamma)$ are at least as big as for the Young's modulus. Otherwise, there may be problems with localized pull-in similar to the problems appearing in dynamic and self-weight problems [26,27]. We use $n = 3$ for all examples. The ratio $\tilde{\varepsilon}_s/\varepsilon_a$ is fixed to 10^5 which is sufficiently large to satisfy the equal potential condition on the surfaces of conductors.

4.2. Local optima issue

As we are dealing with nonlinear multiphysics systems, we observe many local optima and instabilities on the mesh-scale. Consequently, the present results are not global optima and other designs may be obtained with different settings. By comparing objective functions, the results presented are the best ones obtained for a number of different starting guesses and parameter settings.

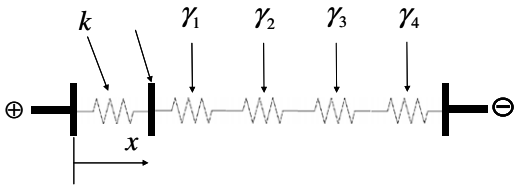

Fig. 13. A simple 1D optimization problem. The goal is to maximize the displacement at A. Optimal designs are $\gamma = (0,1,1,1)$, $(1,0,1,1)$, $(1,1,0,1)$ or $(1,1,1,0)$.

To illustrate the problem of multiple local minima, we consider the optimization problem in Fig. 13. The goal is to maximize the work performed on the left spring with stiffness k. There are four design variables γ_i that can take values 0 or 1 denoting air or material, respectively. Since the electrostatic force and the displacement at A are maximized for minimum gap size, the ith optimal design will be one for all design variables except zero for the ith design variable. Even for this simple 1D example the number of local optima equals the number of finite elements. This problem is even worse for 2D problems.

4.3. Implementation

The monolithic modeling approach and the topology optimization algorithm are implemented in the commercial FE-package COMSOL which is called from a MATLAB script. In this environment, a semi-automated analytical sensitivity analysis using the adjoint method can be easily implemented as described in Refs. [5,10]. The Method of Moving Asymptotes (MMA) is used as the optimizer for all examples [28]. For the first examples we use the sensitivity filter [2] to regularize the design problems.

5. Topology optimization examples

5.1. Numerical example 1 – displacement minimization for electromechanically coupled system

For the first numerical example, we consider the displacement minimization problem shown in Fig. 14. The goal is to optimize the reinforcement on top and bottom of a fixed beam in order to minimize the displacement of point A. As a reference problem we solve an equivalent purely mechanical problem with fixed distributed load at the bottom edge of the fixed beam. The optimization problem for both cases may be written as,

$$\begin{aligned} &\text{Min} && \Phi = v_a^2, \\ &\text{subject to} && M \leqslant M_0, \end{aligned} \tag{45}$$

where M and M_0 are the actual and the allowable mass, respectively.

Fig. 15 shows the optimized designs considering electrostatic force and equivalent pure structural pressure as a reference. The design including electromechanical coupling in Fig. 15a only fills little of the lower design domain with material to avoid building up extra electrostatic forces which are inversely proportion to the second power of the gap distance. The stiffener in the left part of the lower design domain appears because advantage in stiffness exceeds disadvantage in electrostatic force. For the purely structurally loaded beam in Fig. 15b, there is no penalization from introducing material in the lower part of the design domain. Hence, the obtained structure is much stiffer than for the electromechanically coupled beam. But as expected, the objective function of Fig. 15b considering the electromechanical coupling is 21 times higher than that of the design of Fig. 15a. This example clearly shows the importance of considering electromechanical coupling in the design.

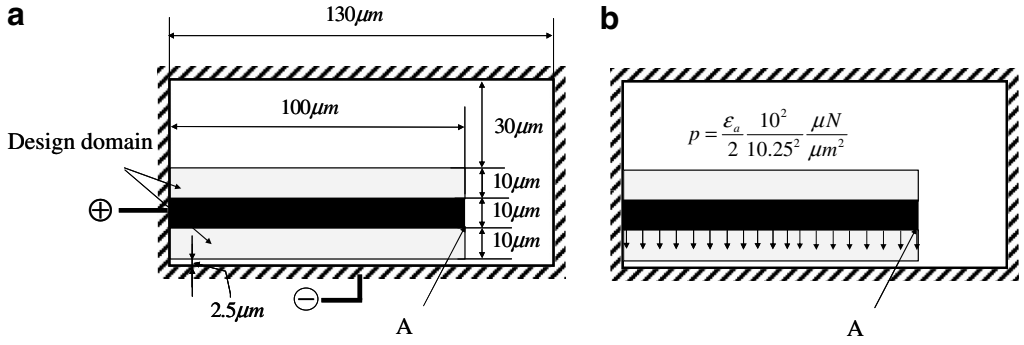

Fig. 14. Displacement minimization problem (Young's modulus of solid: 153 GPa, Poisson's ratio of solid: 0.17, relative permittivity of solid: 10, relative permittivity of air: 1, volume constraint: 30%, applied voltage: 10 V). (a) Problem definition considering electromechanical coupling and (b) problem definition with pure structural pressure.

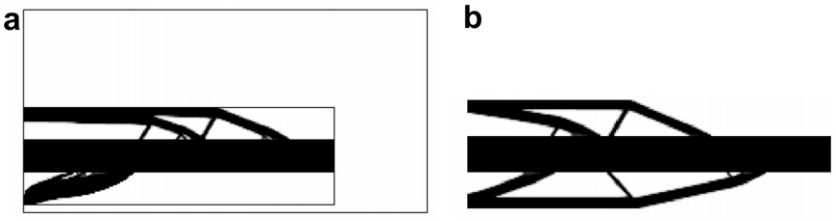

Fig. 15. Optimization results for the design problems in Fig. 14. (a) An optimized design considering electromechanical coupling ($\Phi = 9.4719 \times 10^{-14}$ μm^2) and (b) an optimized design for purely mechanical modeling ($\Phi = 2.0534 \times 10^{-12}$ μm^2 considering electromechanical coupling).

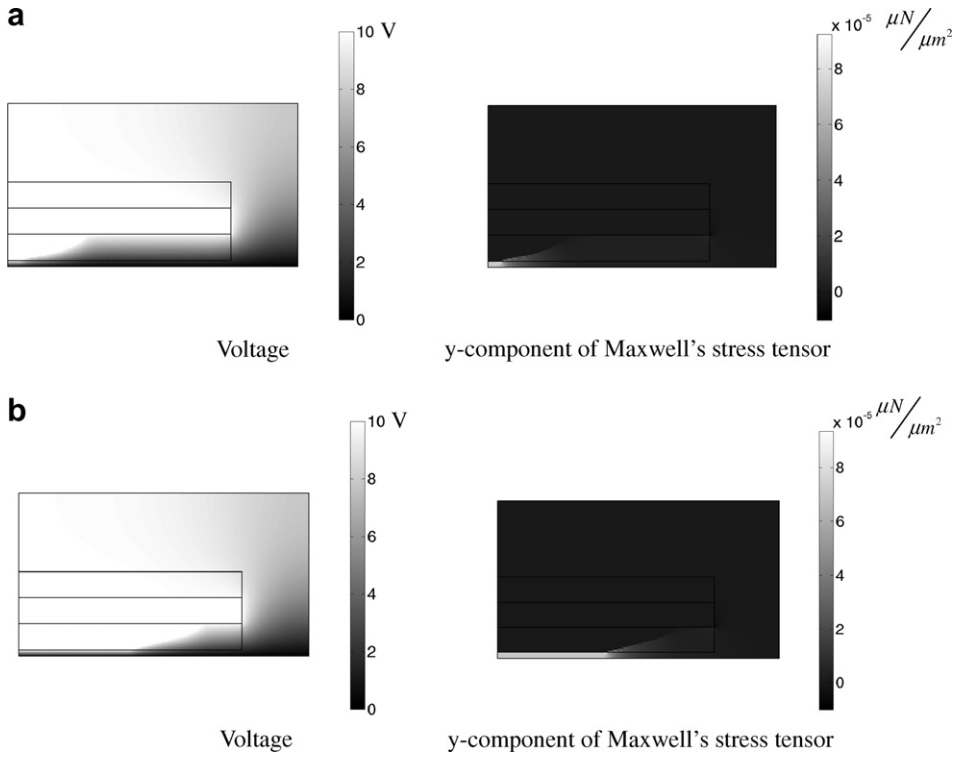

Fig. 16. Voltage and electric Maxwell's stress tensor of Fig. 15. (a) Voltage and *y*-component of Maxwell's stress tensor of Fig. 15a, and (b) voltage and *y*-component of Maxwell's stress tensor of Fig. 15b.

Fig. 16 shows the voltage distribution and the *y*-component of Maxwell's stress tensor for the optimized designs from Fig. 15. It is observed that the potential is constant (white) within the structural parts and that the area with large *y*-component of Maxwell's stress tensor in Fig. 15b is larger.

5.2. Numerical example 2 – inverter design

5.2.1. Force inverter design with a predefined air gap

As a second numerical example we consider the micro force-inverter shown in Fig. 17 [11]. The objective function is to maximize the force applied to the output spring (k_s) which simulates a work piece and again there is a constraint on the mass:

$$\begin{aligned} &\text{Min} && \Phi = -k_s \cdot v_A, \\ &\text{subject to} && M \leqslant M_0, \end{aligned} \tag{46}$$

where v_A is the vertical displacement of point A.

Because of the predefined air gap between the design domain and the bottom electrode, most of the electrostatic force will be developed here. Therefore, it is reasonable to compare the optimized design with one obtained considering purely mechanical pressure as shown in Fig. 17b. Fig. 18 shows the designs obtained using the two design problem definitions. The two layouts and their objective functions are very similar.

5.2.2. Force inverter design without a predefined air gap

In the previous example, we among others found the following:

1. Not surprisingly, topology optimization considering purely mechanical loads can be used for electrostatic systems having predefined air gaps.
2. If there is a predefined air gap, direction, magnitude, and actuation area of electrostatic forces are fixed. Therefore, if the objective is to find optimized designs with predefined air gaps, we do not have to use the present monolithic approach.

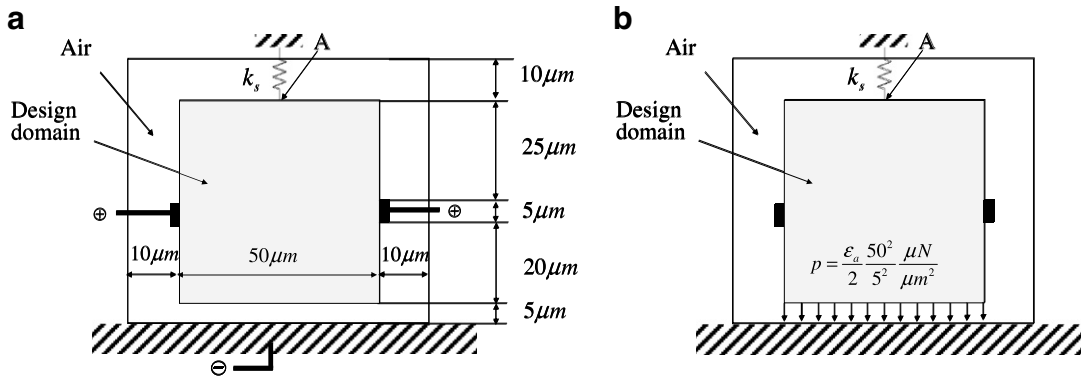

Fig. 17. Problem definition for the electrostatic force inverter design. (Young's modulus of solid: 153 GPa, Poisson's ratio of solid: 0.17, relative permittivity of solid: 10, relative permittivity of air: 1, the spring constant: k_s = 40 μN/μm, mass constraint: 30%, applied voltage: 50 V). (a) Design domain with a predefined 5 μm air gap and (b) a purely mechanical design problem as a reference.

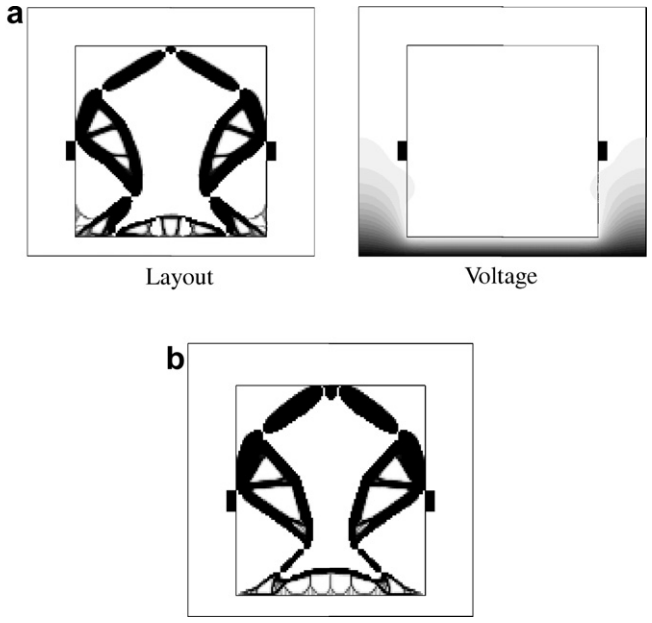

Fig. 18. Optimized designs for the force inverter example with a fixed air gap. (a) An optimized design considering electrostatic loads ($\Phi = -0.0346$ μN), and (b) an optimized design considering purely structural loads ($\Phi = -0.0389$ μN and $\Phi = -0.0421$ μN considering electromechanical coupling).

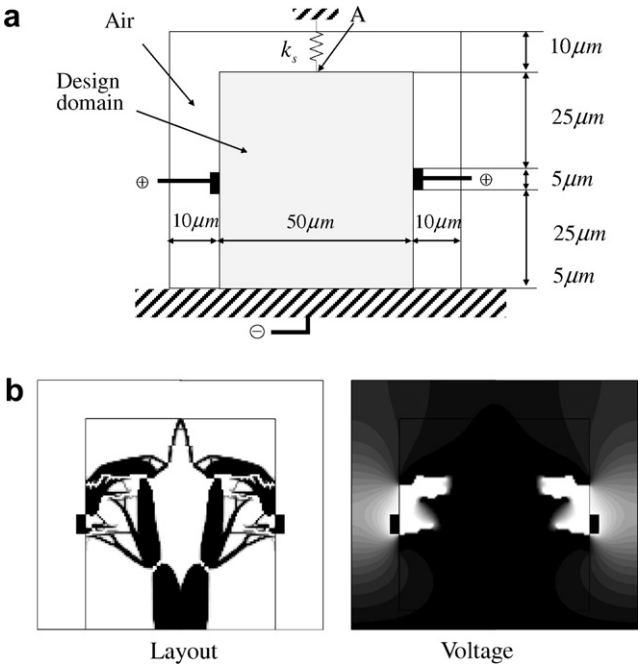

Fig. 19. An optimization without a predefined air gap. (a) Design domain and (b) an optimized design with objective function $\Phi = -1.5833$ μN and voltage distribution.

Hence, it is of more interest to consider an optimization problem without the predefined air gap as shown in Fig. 19a. Without the predefined air gap, electrode area, direction and magnitude of electrostatic force should be optimized. This case can only be solved using the suggested monolithic approach. Fig. 19b shows the resulting optimized design. In terms of objective function, this design is superior to the design in Fig. 18a. However, the mechanical behavior of the actuator is difficult to understand because of the intricate electrodes patterns that appear in the entire design domain. Also, the electrode gaps are determined by the size of the elements – i.e., an obvious and strong mesh-dependence since the actuation force is proportional to the inverse of the square of the gap size.

These problems may be solved by two means. First we present a simple but heuristic method to limit the actuation area by manipulating the Permittivity of the linear elasticity equation as shown in Eq. (47). The idea is that we define an actuation area Ω_A inside the design domain where the electrostatic force may be developed. The Maxwell's stress tensor is set to zero outside the actuation window by the filter function $\Psi(\mathbf{x})$ defined in Eq. (49). If the actu-

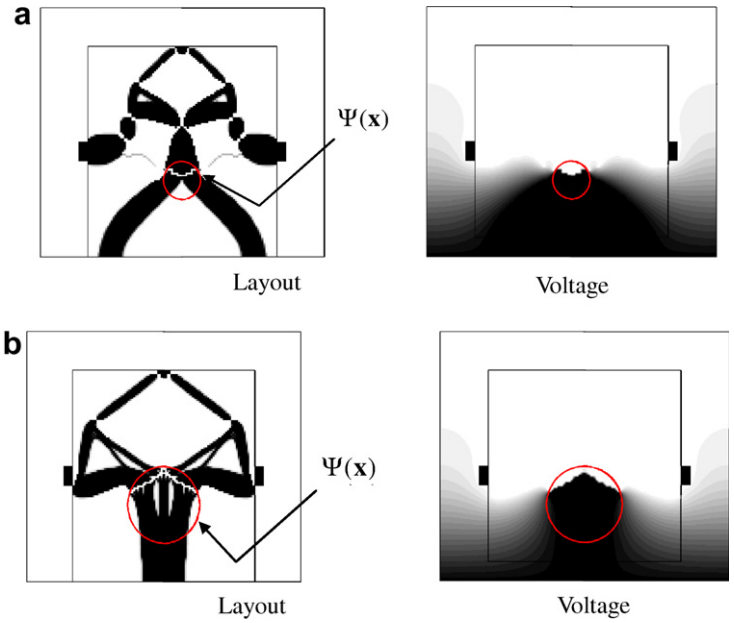

Fig. 20. Design examples with the circular actuation window at the bottom of design domain. (a) An optimized design having 5 μm radius for $\Psi(\mathbf{x})$ ($\Phi = -0.4610$ μN, $\Phi = -0.5226$ μN without $\Psi(\mathbf{x})$) and (b) and optimized design having 10 μm radius for $\Psi(\mathbf{x})$ ($\Phi = -0.7172$ μN, $\Phi = -0.7331$ μN without $\Psi(\mathbf{x})$).

ation window equals the design domain, it corresponds to the previously solved problems. Using this window Ω_A, we limit the actuation area for electrostatic forces but not the direction of the electrostatic force:

$$\int_{0_\Omega} \delta \mathbf{S}^{\mathrm{T}} \cdot \mathbf{T} \mathrm{d}\Omega = -\int_{t_\Omega} \delta \mathbf{S}(\mathbf{u}, \delta \mathbf{u})^{\mathrm{T}} \cdot \tilde{\mathbf{T}}_E \mathrm{d}\Omega, \tag{47}$$

$$\tilde{\mathbf{T}}_E = \Psi(\mathbf{x}) \mathbf{T}_E, \tag{48}$$

$$\Psi(\mathbf{x}) = \begin{cases} 1 & \mathbf{x} \in \Omega_a, \\ 0 & \mathbf{x} \notin \Omega_a. \end{cases} \tag{49}$$

The size and position of the window can be empirically chosen considering manufacturability and design space limits. For example, if there are some specific areas where actuation is not allowed inside a MEMS actuator design domain, window number, size and position can be selected accordingly. A risk associated with the use of the actuation window is that important electrostatic forces may be ignored. For the following examples, however, this does not appear to be a problem.

Fig. 20 shows the optimized designs for two different actuation windows denoted by circles. Obviously, the objective functions with the filtered Permittivities are lower than that of Fig. 19, but we obtain much clearer designs.

5.2.3. Feature size control using a morphology based filter

The previously presented inverter designs have been physically questionable since gap sizes equal element sizes and hence the numerical results cannot be trusted. Also, the optimized designs will be difficult to manufacture due to intricate and small details. The mentioned problems can probably not be resolved by simple postprocessing of the designs since even small changes in the gap regions will affect the performance drastically. Therefore, it is better to introduce a minimum length-scale in the design process by a filtering method.

There are two main kinds of filters in structural optimization. So far we used the sensitivity filtering method that modifies sensitivities by averaging over neighboring elements. Another kind of filter is the density filter which averages densities over neighboring elements. Clearly, the sensitivity filter is not capable of controlling gaps for the present design problem. Apparently, the gain obtained in objective function for small gap sizes exceeds the filtering effect.

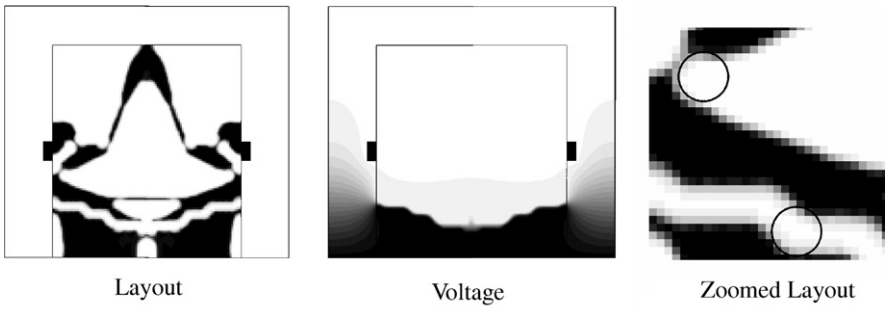

Fig. 21. An optimized design using the erode filter (r_{filter} = 1.6 μm, Φ = −0.2974 μN).

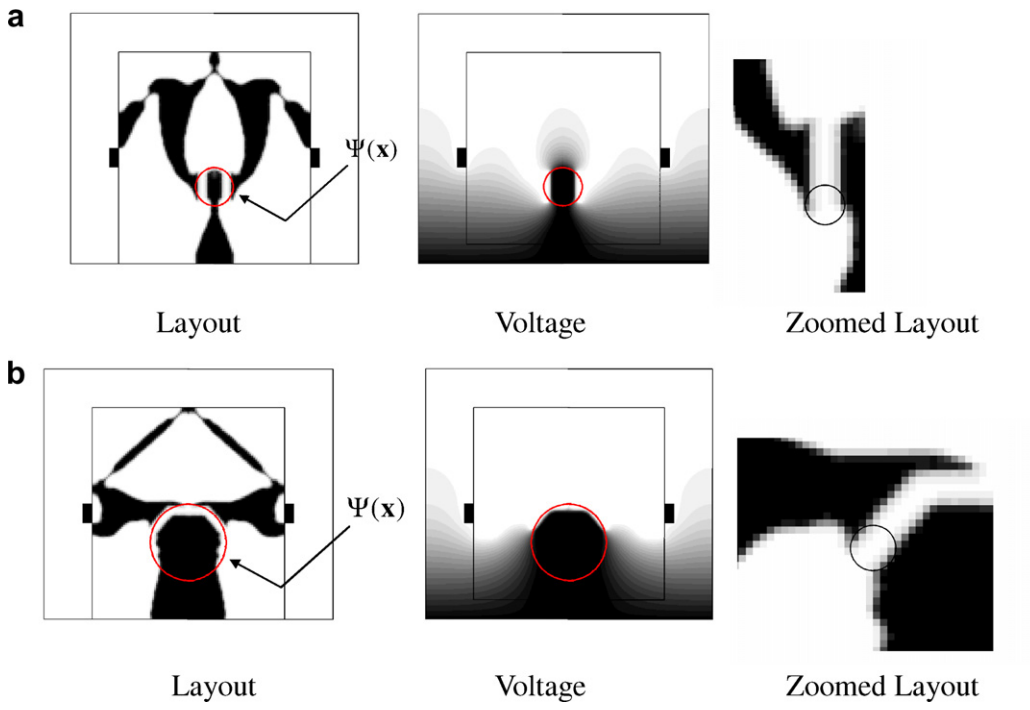

Fig. 22. Design examples with the circular actuation window and the erode filter (r_{filter} = 1.6 μm). (a) An optimized design having 5 μm radius for Ψ(**x**) (Φ = −0.2518 μN, Φ = −0.2589 μN without Ψ(**x**)) and (b) an optimized design having 10 μm radius for Ψ(**x**) (Φ = −0.2538 μN, Φ = −0.2559 μN without Ψ (**x**)).

A new type of density filters called morphological filters based on the density filter was recently proposed in [29]. The morphology filters overcome problems with grey transition zones seen for conventional filters. The basic idea of these filters is to employ image processing operators such as Erode and Dilate to ensure feature size control without grey transition regions. Here we use the erode filter which is good in preventing holes (and gaps) with features smaller than the filter radius (r_{filter}). The erode filter defines the density of the center element to be the minimum of the densities of the neighboring elements. However, in order to obtain a differentiable function the min operator is converted to a continuous one using a Kreisselmeier-Steinhauser formulation:

$$\tilde{\rho}_e = 1 - \log\left(\frac{\sum_{i\in\mathbf{N}_e} e^{\beta(1-\rho_i)}}{\sum_{i\in\mathbf{N}_e} 1}\right)\Big/\beta, \tag{50}$$

where $\tilde{\rho}_e$ is the eth filtered density which is used for the analysis and $\mathbf{N}_e$ is the index of the neighbor elements. Using a continuation method, β is gradually increased during the optimization iterations as suggested in [29]. Remark that for β close to zero, the filter corresponds to the usual density filter with equal weighs and as β increases it approaches the min operator.

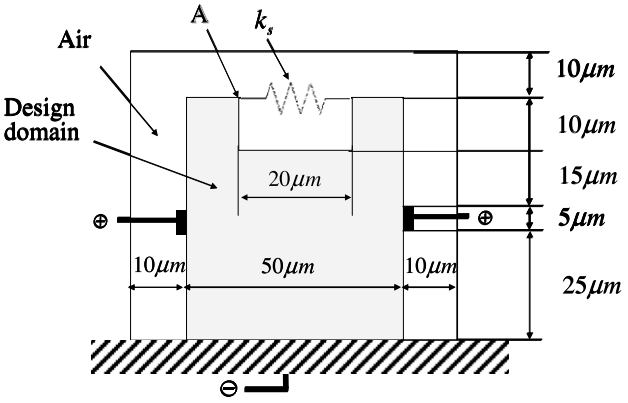

Fig. 24. Problem definition for the electrostatic gripper design. (Young's modulus of solid: 153 GPa, Poisson's ratio of solid: 0.17, relative permittivity of solid: 10, relative permittivity of air: 1, the spring constant: $k_s = 20$ μN/μm, mass constraint: 30%, applied voltage: 50 V).

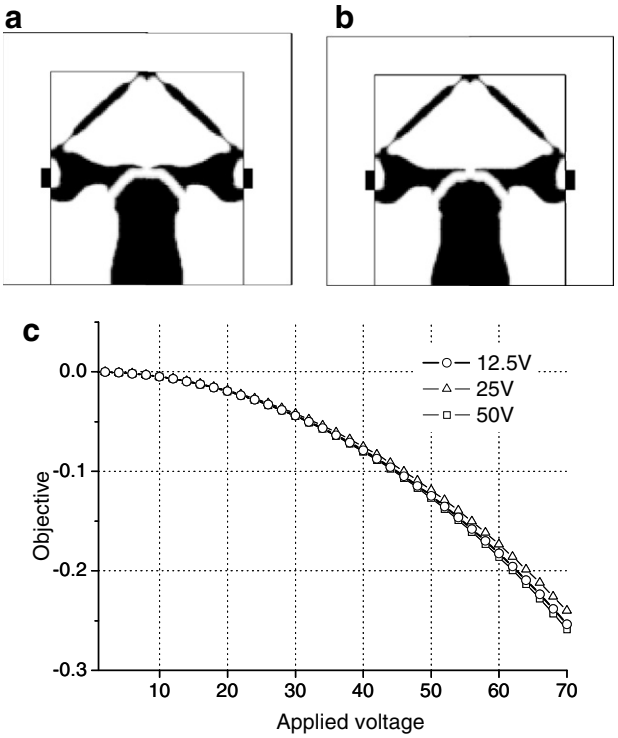

Fig. 23. Affect of applied voltage. (a) A layout with 12.5 V, (b) a layout with 25 V, and (c) responses of these designs with respect to voltage.

In Fig. 21, we use the erode filter ($r_{\text{filter}} = 1.6$ μm) for the inverter design without a prescribed air gap. As seen, the erode filter provides a simpler design compared to the design in Fig. 19 and most importantly, the gap size no longer corresponds to one element but rather to two times the filter radius as seen in the insert of Fig. 21. In Fig. 22, we solve the problem with the zone control as well as the morphology filter and also here we observe mesh-independent feature sizes.

5.2.4. Voltage effects

To study the effect of the applied voltage, we rerun the example from Fig. 22b with 12.5 V and 25 V as actuation voltages. The resulting topologies are seen in Fig. 23. The topological differences are hard to see and in the objective function vs. actuation voltage graph in Fig. 23c, it is noted that also the performances only change slightly for the three different designs. For larger actuation voltages such as 100 V, we experience pull-in effects that hinder convergence.

5.3. Numerical example 3 – Gripper design

As a final example, we consider the gripper design problem sketched in Fig. 24. Here the goal is to maximize the work performed on the horizontal spring. The resulting design obtained using the erode filter is seen in Fig. 25. Again we can observe that the gap size is defined by the filter size and that the method is efficient in optimizing electromechanical actuators.

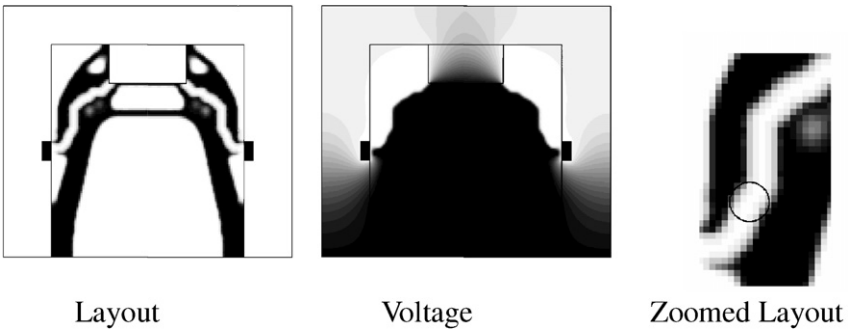

Fig. 25. An optimized design with the erode filter ($r_{\text{filter}} = 1.6$ μm, $\Phi = -0.1271$ μN).

6. Conclusions

This paper suggests a topology optimization procedure for electromechanically coupled systems including design dependent electrostatic loads. First of all, unlike in standard structural optimization problems, alternating governing equations become an important issue. The electric equation and the linear elasticity equation for structural displacements must be interpolated in between depending on design variables. Moreover, the efficient implementation of the interaction boundary conditions also becomes an important issue.

To resolve these issues in topology optimization, we derive a new monolithic formulation from continuum mechanics. The key point of the idea is that the electric and elastic fields are computed in both air and conductor. The coupling between the two governing equations in the deformed domain is achieved by transforming the differential operators from the deformed domain to the undeformed domain and vice versa using the deformation tensor. Moreover, to satisfy the equal potential condition on surfaces of conductors, we introduce a generalized Permittivity formulation for the electric equation. By assigning a high generalized-Permittivity value for the conductor, we can satisfy the equal potential condition on its surface.

The validity of the proposed approach is verified by simple one-dimensional analysis examples and by solving complex MEMS inspired topology optimization problems. The method is prone to local minima and is strongly mesh-dependent. We avoid these issues, partly by introducing an "actuation windows" inside the design domain which restricts the actuation area and partly by use of image-morphology based erode filtering that sets a minimum size constraint for gap sizes.

With this paper we believe that we have paved the way for solving problems involving complicated multi-physics couplings involving boundary dependent loads. As suggestions for future work we suggest to include pull-in voltage and geometrical nonlinearities. This will make the resulting structures more realistic and reliable. Also, it will be interesting to apply the idea to other multiphysics problems with design dependent loads.

Acknowledgements

This research project was supported by the Hans Christian Ørsted Programme of the Technical University of Denmark (GHY), by the Eurohorcs/ESF European Young Investigator Award (EURYI) through the Grant "synthesis and topology optimization of optomechanical systems" (OS) and by the Danish Center for Scientific Computing (DCSC).

References

[1] M.P. Bendsøe, N. Kikuchi, Generating optimal topologies in structural design using a homogenization method, Comput. Methods Appl. Mech. Engrg. 71 (1988) 197–224.
[2] M.P. Bendsøe, O. Sigmund, Topology Optimization Theory, Methods and Applications, Springer-Verlag, New York, 2003.
[3] O. Sigmund, Design of multiphysics actuators using topology optimization – part I: one material structure, Comput. Methods Appl. Mech. Engrg. 190 (49–50) (2001) 6577–6604.
[4] G.H. Yoon, Y.Y. Kim, The element connectivity parameterization formulation for the topology design optimization of multiphysics systems, Int. J. Numer. Methods Engrg. 64 (2005) 1649–1677.
[5] G.H. Yoon, J.S. Jensen, O. Sigmund, Topology optimization of acoustic-structure interaction problems using a mixed finite element formulation, Int. J. Numer. Methods Engrg. 70 (2007) 1049–1076.
[6] L.H. Olesen, F. Okkels, H. Bruus, A high-level programming-language implementation of topology optimization applied to steady-state Navier-Stokes flow, Int. J. Numer. Methods Engrg. 65 (7) (2006) 975–1001.
[7] E. Lemaire, P. Duysinx, V. Rochus, J.C. Golinval, Improvement of pull-in voltage of electromechanical microbeams using topology optimization, in: Proceedings of the III European Conference on Computational Mechanics Solids, Structures and Coupled Problems in Engineering, Springer, Berlin, 2006.
[8] V. Rochus, D.J. Rixen, J.C. Golinval, Monolithic modelling of electro-mechanical coupling in micro-structures, Int. J. Numer. Methods Engrg. 65 (2006) 461–493.
[9] Z. Liu, G.K.J.G. Korvink, M.L. Reed, Multiphysics for structural topology optimization, Sensor Lett. 4 (2) (2006) 191–199.
[10] O. Sigmund, P.M. Clausen, Topology optimization using a mixed formulation: an alternative way to solve pressure load problems, Comput. Methods Appl. Mech. Engrg. 196 (13–16) (2007) 1874–1889.
[11] M. Raulli, K. Maute, Topology optimization of electrostatically actuated microsystems, Struct. Multidiscip. Optim. 30 (5) (2005) 342–359.
[12] J.K. Byun, I.H. Park, S.Y. Hahn, Topology optimization of electrostatic actuator using design sensitivity, IEEE Trans. Magn. 38 (2) (2002) 1053–1056.
[13] T. Borrvall, J. Peterson, Topology optimization of fluids of stokes flow, Int. J. Numer. Methods Fluids 41 (2003) 77–107.
[14] Yin Luzhong, G.K. Anathasuresh, A novel topology design scheme for the multiphysics problems of electro-thermally actuated compliant micromechanisms, Sensors Actuators A 97–98 (2002) 599–609.
[15] A. Alwan, G.K. Ananthasuresh, Topology optimization of electrostatically actuated micromechanical structures with accurate electrostatic modeling of the interpolated material model, Proceedings of the ASME Design Engineering Technical Conference, DETC2006–99684, 2006.
[16] G.H. Yoon, O. Sigmund, Topology optimization for electrostatic system, in: Proceedings of the WCSMO7 – May, Korea, 2007.
[17] P.F. Isabelle Harouche, C. Shafai, Simulation of shaped comb drive as a stepped actuator for microtweezers application, Sensors Actuators A 123–124 (2005) 540–546.
[18] J.H. Kuang, C.J. Chen, The nonlinear electrostatic behavior for shaped electrode actuators, Int. J. Mech. Sci. 47 (2005) 1172–1190.
[19] W. Ye, S. Mukherjee, N.C. MacDonald, Optimal shape design of an electrostatic comb drive in microelectromechanical systems, J. Microelectromech. Syst. 7 (1) (1998) 16–26.
[20] B.D. Jensen, K. Kurabayashi, Shaped comb fingers for tailored electromechanical restoring force, J. Microelectromech. Syst. 12 (3) (2003) 373–383.
[21] David K. Cheng, Field and Wave Electromagnetics, Addison-wesley publishing, New York, 1989.
[22] ANSYS User's Manual, Swanson Analysis Systems, Inc., Houston. PA, 1995.
[23] K.J. Bathe, Finite Element Procedures, Prentice-Hall, New Jersey, 1996.
[24] T. Belytschko, W.K. Liu, B. Moran, Nonlinear Finite Elements for Continua and Structures, John Wiley, New York, 2000.
[25] COMSOL Reference Manual, COMSOL, 2007.
[26] N.L. Pedersen, Maximization of eigenvalues using topology optimization, Struct. Multidiscip. Optim. 20 (1) (2000) 2–11.
[27] M. Bruyneel, P. Duysinx, Note on topology optimization of continuum structures including self-weight, Struct. Multidiscip. Optim. 29 (4) (2004) 245–256.
[28] K. Svanberg, The method of moving asymptotes – a new method for structural optimization, Int. J. Numer. Methods Engrg. 24 (1987) 359–373.
[29] O. Sigmund, Morphology-based black and white filters for topology optimization, Struct. Multidiscip. Optim. 33 (4–5) (2007) 401–424.